

EgoBody: Human Body Shape, Motion and Social Interactions from Head-Mounted Devices

Siwei Zhang¹ Qianli Ma¹ Yan Zhang¹ Zhiyin Qian¹ Marc Pollefeys^{1,2} Federica Bogo² Siyu Tang¹
¹ETH Zürich ²Microsoft

{siwei.zhang, qianli.ma, yan.zhang, marc.pollefeys, siyu.tang}@inf.ethz.ch
 zhqian@ethz.ch febogo@microsoft.com



Figure 1. EgoBody is a large-scale dataset for human 3D motion and social interactions in 3D scenes. Given two interacting subjects, we leverage a lightweight multi-camera rig to reconstruct their 3D shape and pose over time (top row). One of the subjects (blue) wears a head-mounted device, synchronized with the rig, capturing egocentric multi-modal data like eye gaze tracking (red circles in middle row) and RGB images (bottom). Note that data with visible faces will be released.

Abstract

Understanding social interactions from first-person views is crucial for many applications, ranging from assistive robotics to AR/VR. A first step for reasoning about interactions is to understand human pose and shape. However, research in this area is currently hindered by the lack of data. Existing datasets are limited in terms of either size, annotations, ground-truth capture modalities or the diversity of interactions. We address this shortcoming by proposing EgoBody, a novel large-scale dataset for social interactions in complex 3D scenes. We employ Microsoft HoloLens2 headsets to record rich egocentric data streams (including RGB, depth, eye gaze, head and hand tracking). To obtain accurate 3D ground-truth, we calibrate the headset with a multi-Kinect rig and fit expressive SMPL-X body meshes to multi-view RGB-D frames, reconstructing 3D human poses and shapes relative to the scene. We collect 68 sequences, spanning diverse sociological interaction categories, and propose the first benchmark for 3D full-body pose and shape estimation from egocentric views. Our dataset and code will be available for research at <https://sanweiliti.github.io/egobody/egobody.html>.

1. Introduction

Social interactions play a central role in our life. We constantly interact and communicate with each other; understanding how our social partners move, their intentions and emotions is something almost instinctive for us. However, the same does not hold for machines. Automated perception of the body pose and shape of, and interactions with, a social partner (*i.e.* “second person”) from egocentric views is a very challenging problem, which is far from being solved. Addressing it is crucial for many applications, ranging from assistive robotics to Augmented and Virtual Reality (AR/VR). Despite its importance, the problem has received much less attention in the literature than its “third-person view” counterpart. While there is a large number of methods for full-body pose estimation from RGB(D) frames [10, 14, 23, 33, 34, 36, 39, 49, 58, 67, 78, 81, 86–89], only a few of them address the challenges encountered in images captured from head-mounted devices (HMD). Any method aiming at understanding the poses of the “second person” must deal with severe body truncations, motion blur (exacerbated by the embodied movement of the HMD), people entering/exiting the field of view, to name a few.

A reason for this limited attention is the lack of data. Most human motion datasets do not provide egocentric frames [16, 23, 27, 30, 31, 52, 71, 90], and most capture only one subject at a time [23, 27]. On the other hand, existing egocentric human motion datasets have limitations in terms of annotations, scale and diversity [22, 47, 55, 69, 70, 80, 85]. Some contain only 2D ground-truth, and/or coarse-level interaction labels [15, 45, 54, 60, 65]. The You2Me dataset [55] collects egocentric RGB frames annotated with 3D skeleton joints, without 3D scene context. HPS [22] provides pseudo ground-truth 3D body meshes for the camera wearer, considering very limited social interactions; without using external cameras, the reconstructed motion exhibits jitter and foot skating. Notably, while most existing datasets provide only RGB streams, we use state-of-the-art devices to capture richer, multi-modal data.

To fill this gap, we propose EgoBody, a large-scale egocentric social interaction dataset. We focus on 2-person interaction cases, and pay special attention to the richness and diversity of our interaction scenarios based on the social interaction categories studied in sociology [5] (*cooperation, social exchange, conflict, coercion and conformity*). EgoBody collects egocentric multi-modal data, with accurate 3D human shape, pose and motion ground-truth. Furthermore, EgoBody includes accurate 3D scene reconstructions, providing a holistic and consistent 3D understanding of the physical world around the camera wearer.

The egocentric data is captured with a Microsoft HoloLens2 headset [3], which provides rich multi-modal streams: RGB, depth, head, hand and eye gaze tracking, correlated in space and time. In particular, eye gaze carries vital information for social interactions. By providing eye tracking information synchronized with other modalities, EgoBody opens the door to study relationships between human attention, social interactions and human motions.

The high-quality 3D human shape and motion annotations are obtained with a marker-less motion capture approach. We calibrate and synchronize the HoloLens2 with a multi-camera rig consisting of 3 Azure Kinects [1]. This lightweight setup, easy to deploy in different environments, captures multi-view data which we leverage to get ground-truth annotations in an automated way. Namely, we extend the LEMO framework [89], originally proposed for monocular RGB-D videos, to our setup: we fit the SMPL-X body model [58] to multi-view RGB-D data, reconstructing accurate 3D full-body meshes for both the camera wearer and their interaction partner.

We evaluate several state-of-the-art 3D human pose and shape estimation methods on the EgoBody test set, highlighting its novel, unique challenges, and gaining insights for building more robust approaches that better suit egocentric scenarios. By fine-tuning two recent methods [29, 39] on our training set, we improve their performance on *both*

our test set and the You2Me dataset [55], demonstrating the effectiveness of our training set in helping the models address the challenges posed by the egocentric view data.

Contributions. In summary, our contributions are as follows: (1) we provide the first large-scale egocentric social interaction dataset, EgoBody, with rich and multi-modal data, including first-person RGB videos, eye gaze tracking of the camera wearer, various 3D indoor environments with accurate 3D mesh reconstructions, spanning diverse interaction scenarios; (2) we provide high-quality 3D human shape, pose and motion ground-truth for both camera wearers and their interaction partners by fitting expressive SMPL-X body meshes to the multi-view RGBD videos that are carefully synchronized and calibrated with the HoloLens2 headset; (3) we provide the first benchmark for 3D human pose and shape estimation of the *second person* in the egocentric view during social interactions.

We will provide a benchmark suite and make our dataset, code and models freely available for research purposes.

2. Related Work

Datasets for 3D human motion and interactions. A large number of datasets focus on 3D human pose and motion from *third-person* views [16, 23, 27, 30, 31, 43, 52, 57, 71, 74, 75, 84, 90]. For example, Human3.6M [27] and AMASS [51] use optical marker-based motion capture to collect large amounts of high-quality 3D motion sequences; they are limited to constrained studio setups and images – when available – are polluted by marker data. PROX [23] performs marker-less capture of people moving in 3D scenes from monocular RGB-D, without considering human-human interactions. The quality of the reconstructed motion is further improved by LEMO [89]. The Panoptic Studio dataset [30–32, 79] reconstructs interactions between people using a multi-view camera system; it provides annotations for body and hand 3D joints plus facial landmarks. CHI3D [16] focuses on close human-human contacts, using a motion capture system to extract ground-truth 3D skeletons. 3DPW [74] reconstructs both the 3D shape and motion of people “in-the-wild” by fitting SMPL [48] to IMU data and RGB images captured with a hand-held camera, without reconstructing the 3D environment.

Among datasets for *egocentric* vision, a lot of attention has been put on hand-object interactions and action recognition, often without 3D ground-truth [12, 35, 42, 45, 54, 60, 62, 65, 83]. Mo2Cap2 [80] and xR-EgoPose [69, 70] provide image-3D skeleton pairs for egocentric body pose prediction, but do not consider multiple-people scenarios. You2Me [55] similarly focuses on egocentric body pose prediction, annotating 3D ground-truth skeletons from image sequences captured with a chest-mounted camera plus external cameras. EgoMoCap [47] analyzes the *second-*

Table 1. Comparison with existing image-based datasets with 3D human pose annotations. “Ego” refers to the first-person view. “Interaction” refers to social interactions, and “Global Config.” refers to global translation and rotation.

Dataset	Frame #	Sub. #	3rd-person View	Ego	Body Mesh	Gaze	3D Scene	Interaction	Global Config.
TNT15 [75]	13k	4	✓		✓				✓
3DPW [74]	51k	7	✓		✓*			✓	
PROX [23]	100k	20	✓		✓*		✓		✓
Panoptic [31]	297k	180+	✓					✓	✓
HUMBI [84]	380k	772	✓		✓*	✓			✓
TotalCapture [71]	1,900k	5	✓						✓
Human3.6M [27]	3,600k	11	✓		✓				✓
Mo2Cap2 [80]	15k	5		✓					
You2Me [55]	150k	10		✓				✓	
HPS [22]	300k	7		✓	✓*		✓		✓
Ours	153k	20	✓	✓	✓*	✓	✓	✓	✓

* Body Mesh defined by parametric body models.

person body pose in outdoor social scenarios. HPS [22] reconstructs the body pose and shape of a subject wearing a head-mounted camera moving in large 3D scene, but with few social interactions. Recently, Ego4D [19] collects a massive amount of egocentric videos for various tasks including action and social behavior understanding, making significant advances in stimulating future research in the egocentric domain. Our dataset is complementary to Ego4D in that we provide 3D human pose and shape ground-truth for the camera wearer and their interaction partner.

Table 1 compares EgoBody with the most related human motion datasets. EgoBody is the first dataset that collects calibrated third- and first-person images, with various social interactions, multi-modal data and rich 3D ground-truth.

3D human pose estimation. The problem of estimating 3D human pose from *third-person* view RGB(D) image data has been extensively studied in the literature – either from single frames [4, 6, 8, 11, 14, 20, 21, 23, 33, 37–41, 44, 46, 53, 56, 58, 66, 68, 72, 76, 78, 81, 88, 91], monocular videos [10, 34, 36, 49, 67, 86, 87, 89] or multi-view camera sequences [13, 17, 26, 32, 63, 77]. SPIN [39] estimates SMPL [48] parameters from single RGB images by combining deep learning with classic optimization frameworks. METRO [46] reconstructs human meshes without relying on parametric body models. Most methods require “full-body” images and therefore lack robustness when parts of the body are occluded or truncated, as is the case with the “*second person*” in egocentric videos. EFT [29] injects crop augmentations in the training data to better reconstruct highly truncated people. PARE [37] explicitly learns to predict body-part-guided attention masks. However, these methods exhibit a significant performance drop when applied to egocentric view data. Our dataset helps fill the performance gap, as we show in Sec. 5.

The problem of *egocentric* pose estimation is receiving growing attention. Most methods estimate the *camera wearer’s* 3D skeleton, based on image data, IMU measurements, scene cues or also body-object interactions [22, 28,

50, 64, 69, 70, 85]. You2Me [55] estimates the camera wearer’s pose given the *second-person’s* pose as an additional interaction cue to image data. On the other hand, Liu et al. [47] estimate the *second-person’s* 3D human pose and shape given egocentric videos in outdoor scenes, with limited interaction diversity. Again, we believe EgoBody data will foster further research in this area.

Egocentric social interaction recognition. Egocentric videos provide a unique way to study social interaction signals. Most methods focus on predicting social interaction types [15, 54, 62, 83]. Ye et al. [82] capture egocentric videos of child-adult interactions from the adult’s view, detecting eye contact between the two persons. We provide ground-truth 3D pose and shape of all interacting subjects for potential new research of more fine-grained learning of social interactions.

3. Building the EgoBody Dataset

EgoBody collects sequences of subjects performing diverse social interactions in various indoor scenes. For each sequence, two subjects are involved in one or more predefined interactions (Sec. 3.1). Their performance is captured from both first- and third-person views. One subject (“*first person*”, the camera wearer) wears a HoloLens2 device, capturing multi-modal egocentric data (RGB, depth, head, hand and eye gaze tracking streams). Their interaction partner, *i.e.* *second person*, does not wear any device. The first person’s HoloLens2 is calibrated and synchronized with three Azure Kinect cameras which capture the interaction from different viewpoints (Sec. 3.2). Based on this multi-view data, we acquire rich ground-truth annotations for all frames, including 3D full-body pose and shape for both interacting subjects and the reconstructed 3D scene (Sec. 3.3). Statistics for EgoBody are reported in Sec. 4.

3.1. Social Interaction Scenarios

Existing egocentric datasets typically subdivide their data into a few action classes [22, 55, 70, 80], *e.g.* “con-

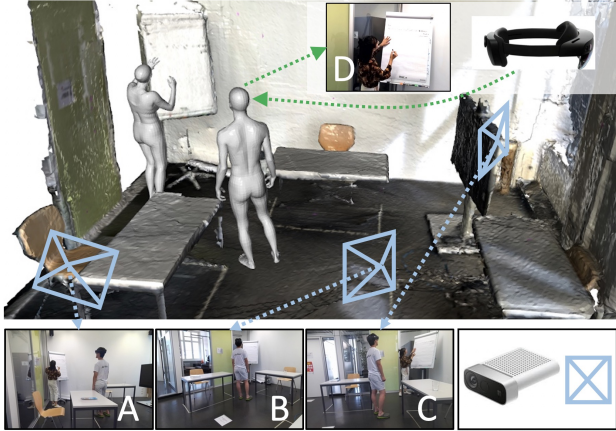


Figure 2. Capture setup. Three Azure Kinets capture the interactions from 3 views (A, B, C), and a synchronized HoloLens2 worn by one subject captures the first-person view image (D).

versation”. In practice we find that instructions based on such broad action classes often lead to monotonous behaviors of subjects. For example, while the category “conversation” includes various scenarios such as “argument”, “self-introduction”, most subjects tend to only go for “self-introduction”, resulting in repetitive emotions and motions. Moreover these action classes are not specifically designed for, hence do not well cover, social interaction scenarios.

To address this, we introduce a more fine-grained classification based on four major interaction categories as defined in sociology studies [5]: *cooperation*, *social exchange*, *conflict* and *conformity*. Within each category we define a set of specific interaction scenarios, see Tab. 2.

For each sequence, we define one or more interactions scenarios and ask the two participants to interact accordingly. Note that we allow the subjects to improvise within each of our fine-grained interaction scenario, thereby ensuring the intra-class variation and naturalness of motions. Sampling interactions from diverse social categories helps us span many action types (Tab. 2). The capture of these interactions in various 3D scenes further incorporates human-scene interactions and increases human motion diversity.

3.2. Data Acquisition Setup

As mentioned above, EgoBody collects first- and third-person view multi-modal data, plus 3D scene reconstructions. Fig. 2 illustrates our system setup.

First-person-view capture. We use a Microsoft HoloLens2 [3] headset to record egocentric data. By using the Research Mode API [73], we capture RGB videos (1920×1080) at 30 FPS, long-throw depth frames (512×512) at 1-5 FPS, as well as eye gaze, hand and head tracking at 60 FPS. Note that we do not record depth at a higher framerate (AHAT) given the “depth aliasing” problem described in [73]. We observe that captures exhibit

challenges which are typical for limited power-devices, like frame drops and blurry images.

Third-person multi-view capture. We use three Azure Kinect cameras [1] (denoted by $Cam1$, $Cam2$, $Cam3$) to capture multi-view, synchronized RGB-D videos of the interacting subjects. Having multi-view data helps our motion reconstruction pipeline for ground-truth acquisition (Sec. 3.3). The cameras are kept fixed during recording. They capture synchronized RGB frames (1920×1080) and depth frames (640×576), at 30 FPS.

3D scene representation. We pre-scan the environment using an iPhone12 Pro Max running the 3D Scanner app [2]. Scene reconstructions are stored as 3D triangulated meshes, each with $10^5 \sim 10^6$ vertices. We choose this procedure for its efficiency and reconstruction quality.

Calibration and Synchronization. For each Kinect, we extract its camera calibration parameters via the Azure Kinect DK [1]. For the HoloLens2, we get its camera parameters as exposed by Research Mode [73]. We synchronize the Kinets via hardware, using audio cables. Since it is not possible to synchronize HoloLens2 and Kinect in a similar way, we use a flashlight which is visible to all devices as signal for the first frame. Kinect-Kinect and Kinect-HoloLens2 cameras are spatially calibrated using a checkerboard. We use $Cam1$ to define our world coordinate frame origin. Note that once we calibrate the HoloLens2 coordinate frame with $Cam1$ ’s world origin, we can track the headset position, and therefore its cameras, by relying on its built-in head tracker [73]. We also register the 3D scene into the world coordinate frame of $Cam1$, and reconstruct the human body in this space (see also Supp. Mat.).

3.3. Ground-truth Acquisition

Given the RGB-D frames captured with the multi-Kinect rig, our motion reconstruction pipeline estimates, for each frame and each subject, the corresponding SMPL-X body parameters [58]. Thanks to the Kinect-HoloLens2 synchronization, this provides accurate per-frame pose, natural human motion dynamics and realistic human-scene interactions for both first- and third-person view frames. Our pipeline builds on LEMO, the multi-stage optimization framework proposed in [89]. LEMO reconstructs temporally consistent human motions in 3D scenes from monocular RGB-D videos by relying on data-driven motion priors. Here we extend the approach to our multi-view, heterogeneous camera setup. Note that we always estimate the body in the coordinate frame of $Cam1$. We optimize for each of the two subjects separately.

SMPL-X Body Model. We use SMPL-X [58], which represents the body as a function $\mathcal{M}_b(\gamma, \beta, \theta, \phi)$. It maps global translation $\gamma \in \mathbb{R}^3$, body shape $\beta \in \mathbb{R}^{10}$, pose θ and facial expression $\phi \in \mathbb{R}^{10}$ to a triangle body mesh

Table 2. EgoBody interaction scenarios.

Category	Interaction Scenarios
Cooperation	Guess by Action game, catching and tossing, searching for items
Social exchange	Teaching with the blackboard, teaching to dance, teaching workout actions, giving a lecture / presentation
Conflict	Arguing about a specific topic
Conformity	One subject instructs the other to perform a task
Others	Haggling (seller-buyer), negotiation, promotion, self-introduction, casual chat
Action Types	Talking, walking, greeting, sitting, jumping, exercising, dancing, drinking, reading, lying, catching and tossing, playing games, passing object, etc..

$\mathcal{M}_b = (V_b, F_b)$ with body vertices $V_b \in \mathbb{R}^{10475 \times 3}$ and faces F_b . The pose parameters include body, facial and hand poses. $J(\beta)$ denotes the 3D body joints in the neutral pose, which can then be posed according to a given θ .

Data preprocessing. We use OpenPose [9] to detect 2D body joints in all (Kinect and HoloLens2) RGB frames. OpenPose identifies people in the same image by assigning a body index to each detected person. In general, this works well, but gives false positives which we process afterwards. To extract human body point clouds from Kinect depth frames, we use Mask-RCNN [24] and DeepLabv3 [24]. We manually inspect the data to remove spurious detections (e.g. irrelevant people in the background, and scene objects misdetected as people). We also ensure consistent subject identification across frames and views, and manually fix inaccurate 2D joint detections, mostly due to body-body and body-scene occlusions. See Supp. Mat. for more details.

Per-frame fitting. As in [89], we first run a per-frame fitting stage. Taking (Kinect) depth and 2D joints as input, we estimate the SMPL-X parameters for each subject/frame separately, minimizing an objective function similar to that defined in [23]:

$$E(\beta, \gamma, \theta, \phi) = E_J + \lambda_D E_D + E_{prior} + \lambda_{contact} E_{contact} + \lambda_{coll} E_{coll}, \quad (1)$$

where $\beta, \gamma, \theta, \phi$ are optimized SMPL-X parameters.

We compute the joint error term E_J on multi-view frames as follows. Given the preprocessed OpenPose 2D joints J_{est}^v from the 3 different views ($v \in \{1, 2, 3\}$), E_J minimizes the sum of 2D distances between J_{est}^v and the 2D projection of SMPL-X joints onto camera view v for all views:

$$E_J = \sum_{view\ v} E_{J_v}(\beta, \gamma, \theta, \phi, J_{est}^v, K_v, T_v), \quad (2)$$

where K_v denotes the intrinsics parameters of camera v , and T_v denotes the extrinsics between $Cam\ v$ and $Cam\ 1$. For robustness, we weight the projection error for each joint by the OpenPose detection confidence score. The depth term E_D penalizes discrepancies between the estimated body surface and body depth point clouds for all

views; E_{prior} represents a set of priors on body pose, shape and expression parameters; $E_{contact}$ encourages contact between scene and body surfaces, and E_{coll} penalizes scene-body inter-penetrations. The λ_i s weight the contribution of each term. We refer the reader to [23, 89] for more details.

Temporally consistent fitting. Per-frame fitting gives us a set of reasonable, initial pose estimates, which however are jittery and inconsistent over time. We therefore run a second optimization stage, using LEMO priors [89] to obtain smooth, realistic human motions. In this stage, we take the median body shape β , computed from per-frame fitting results, and do not optimize it further.

We extend the LEMO formulation to the multi-view setting and, differently from the first stage, we consider also egocentric data during optimization. To improve consistency between first- and third-person view estimates, we take OpenPose 2D joint estimates from HoloLens2 RGB frames and use them as further constraints.

The resulting objective function minimized in the temporal fitting stage is:

$$E(\gamma, \theta, \phi) = E_J + E_{J_{fpv}} + E_{prior} + \lambda_{smooth} E_{smooth} + \lambda_{fric} E_{fric}, \quad (3)$$

where E_{fric} is the contact friction term defined in [89] to penalize body vertex velocities when in contact with the scene, E_{smooth} and E_{prior} denote temporal and static priors as in [89]. $E_{J_{fpv}}$ is the 2D projection term which minimizes the error between OpenPose detections on first-person view frames and the 2D projections of SMPL-X joints onto the head camera view; $E_{J_{fpv}}$ is only enabled for the *second person* when he or she is visible in the egocentric view frames. The λ_i s weight balance the contribution of each term.

Multi-view reconstruction accuracy. To evaluate the accuracy of reconstructed human body in the first-person view frames, we randomly select 2,286 frames and manually annotate them via Amazon Mechanical Turk (AMT) for 2D joints following SMPL-X body joint topology (see details in Supp. Mat.). By projecting body joint annotations of our dataset on the egocentric view images, the joint error is computed as the 2D Euclidean distance between the 2D projections and AMT annotations. The mean 2D joint accuracy is 31.28 pixels for images with 1920×1080 resolution.

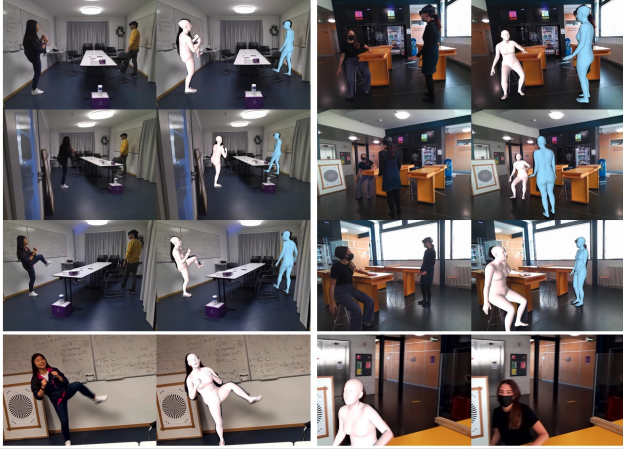


Figure 3. Reconstructed ground-truth bodies overlaid on third-person view images from 3 Kinects (row 1-3), and the first-person view image (row 4). Blue denotes the camera wearer, and pink denotes the *second person*. Left/right shows 2 different frames.

4. EgoBody Dataset

EgoBody collects 68 sequences from 20 subjects (10 male and 10 female) performing diverse social interactions in 9 indoor scenes. In total, there are 153,350 synchronized frames captured from the Azure Kinects, from multiple third-person views. We refer to this as the “Multi-view (MV)Set”. For each MV frame, we provide 3D human full-body pose and shape annotations (as SMPL-X parameters) for both interacting subjects together with the 3D scene mesh. Furthermore, we have 138,686 egocentric RGB frames (the “EgoSet”), captured from the HoloLens, calibrated and synchronized with the Kinect frames. Given the camera wearer’s head motion, the *second person* is not visible in every egocentric frame: in total, we have 114,297 frames where the *second person* is visible in the first-person view (“EgoSet-*second-person*”). Fig. 3 shows example images. For EgoSet, we also collect the head, hand and eye tracking data, plus the depth frames from the HoloLens2.

Training/test splits. We split our data into training and test sets such that they do not have overlapping subjects. The EgoBody training set contains 58,250 MVSet frames, 53,986 Ego-frames and 46,033 EgoSet-*second-person* frames. The test set contains 95,100 MV frames, 84,700 Ego frames and 68,264 Ego-*second-person* frames.

Joint visibility. The camera wearer’s motion, the headset’s field of view and the close distance between the interacting subjects cause the *second person* to be often truncated in the egocentric view. To quantify the occurrences of truncations, we project the fitted 3D body joints onto the HoloLens2 images, and deem a projected 2D joint as “visible” if it lies inside of the image. As shown in Fig. 7(b), lower parts of the body are more frequently truncated in the images, whereas the upper body parts are more visible. Please refer to Sec. 5

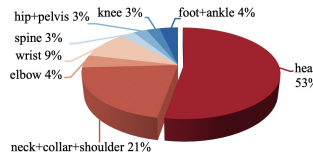


Figure 4. **Which body part attracts attention?** For each joint group, % of the occurrences it is the closest to the 2D gaze point in the image.

for its impact on 3D human pose and shape estimation performance, and Supp. Mat. for more detailed statistics.

Eye gaze and attention. We can combine the HoloLens2 eye gaze tracking information with our 3D reconstruction of the scene/people to calculate the 3D location the user looks at, and project it on the egocentric images. In this way we understand where the user’s “attention” is focused, thereby obtaining valuable data for interaction understanding. In the Supp. Mat., we analyze in detail the relationship between these attention areas and the locations of the *second person*’s body joints in the image. Our observation confirms that the camera wearer’s attention is highly focused on the *second person* during interactions. The subjects’ attention tends to be closer to the upper body joints (Fig. 4), which in turn results in lower visibility for the lower body parts.

Interaction distance. EgoBody covers a large range of indoor interaction distances (the 3D Euclidean distance between the pelvis joint of the interacting subjects), ranging from 0.88m to 4.10m (see the distribution in Supp. Mat.).

5. Experiments

We leverage EgoBody to introduce the first benchmark for 3D human pose and shape (3DHPS) estimation from egocentric images. Given a single egocentric RGB image of a target subject, the goal of a 3DHPS method is to estimate a human body mesh and a set of camera parameters, which best explain the image data.

The performance of state-of-the-art (SoTA) 3DHPS methods is starting to saturate on common datasets [27, 74]; yet, their capabilities to generalize to real-world scenarios (e.g., cropped or blurry images) are still limited [57]. With EgoBody, we can test their capabilities on egocentric images. We define a benchmark for 3DHPS methods on our EgoSet-*second-person* test set. We evaluate several SoTA methods and show that their performance significantly drops on our data. We analyze the results and provide insights to make them more robust and suitable to egocentric scenarios. In particular, we show that our EgoSet-*second-person* training set can help address the challenges in egocentric view data: using it we fine-tune two recent methods, SPIN [39] and EFT [29], achieving improved accuracy on both our test set and the You2Me [55] dataset.

5.1. Benchmark Evaluation Metrics

We employ two common metrics: Mean Per-Joint Position Error and Vertex-to-Vertex errors. We carry out two

Table 3. Evaluation of SoTA 3DHPS estimation methods on our test set. All metrics are in *mm*. “PA-” stands for Procrustes alignment (see Sec. 5.1). “SPIN-ft” and “EFT-ft” denote the result of fine-tuning SPIN and EFT on our training set.

Method	MPJPE ↓	PA-MPJPE ↓	V2V ↓	PA-V2V ↓
CMR [40]	248.7	124.7	289.5	170.3
SPIN [39]	189.9	107.9	210.5	126.0
LGD [66]	162.5	95.9	179.0	113.3
METRO [46]	161.5	91.2	187.5	112.3
PARE [37]	129.9	83.5	145.1	98.3
EFT [29]	123.3	72.9	143.4	87.1
SPIN-ft (Ours)	96.2	58.4	122.3	85.2
EFT-ft (Ours)	92.5	56.1	115.1	79.1

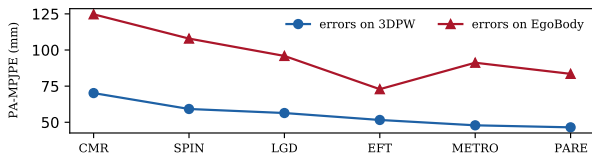


Figure 5. 3D joint errors of SoTAs on 3DPW and our dataset with the advance of the 3DHPS field.

types of alignments before computing the accuracy for each metric: (1) translation-only alignment (aligns the bodies at the pelvis joint [57]) and (2) Procrustes Alignment [18] (“PA”, solves for scale, translation and rotation). Results are by default reported with translation-only alignment unless specified with the “PA-” prefix.

Mean Per-Joint Position Error (MPJPE) is defined as the mean Euclidean distance between predicted and ground-truth 3D joints. We evaluate on 22 body joints from SMPL.

Vertex-to-Vertex (V2V) error is the mean Euclidean distance over all vertices, computed between two meshes with the same topology. For methods that predict SMPL bodies we report V2V errors on the *main body* vertices (*i.e.* body without head, where SMPL and our ground-truth SMPL-X have the same topology).

5.2. Baseline Evaluation

Tab. 3 summarizes the evaluation of SoTA 3DHPS methods from different categories: (1) fitting-based method [66]; and regression-based methods that (2) predict parameters of a parametric body model [29, 37, 39, 40] or (3) directly predict non-parametric body meshes [46]. For each baseline method, we use the best performing model provided by the authors (trained with the optimal training data).

In Fig. 5 we plot the PA-MPJPE error of these methods on our dataset and on an existing major benchmark¹, 3DPW [74]. On average, the methods yield a 74% higher 3D joint error on EgoBody than on 3DPW. More importantly, while the accuracy curve drives towards saturation on 3DPW, different SoTA methods still show largely vary-

¹The results on 3DPW are taken from the respective original papers.

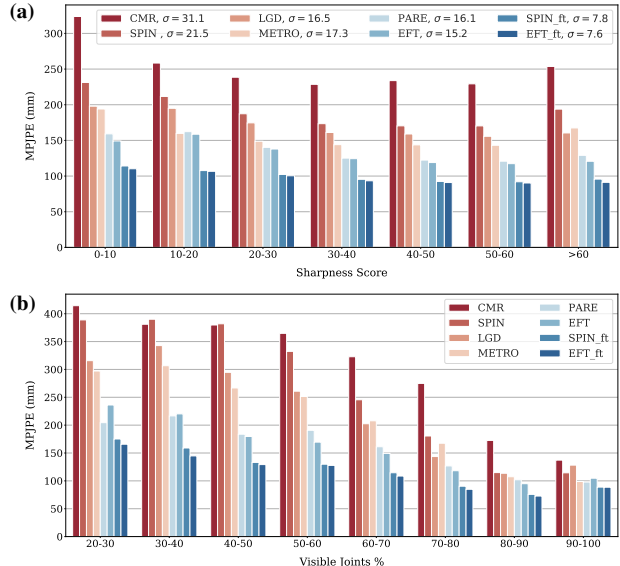


Figure 6. Impact of (a) motion blur and (b) percentage of visible joints on the accuracy of SoTA methods.

ing performance on our dataset. This suggests that current datasets are not sufficient to train models that can handle the first-person view images well. Below we discuss two key challenging factors that impact performance.

Motion blur. Motion blur is common in the first-person view images due to the motion of the camera wearer. To determine how motion blur influences 3DHPS estimation accuracy, we plot in Fig. 6(a) the MPJPE of all methods vs. the image sharpness score. The sharpness score is defined as the variance of the Laplacian of an image [59], upper-thresholded at 60; higher scores mean sharper images (see Supp. Mat. for details). We observe that, surprisingly, most methods are insensitive to image blurriness, except for heavily blurred cases (score <10). However, our fine-tuned models (SPIN-ft / EFT-ft) are more robust against motion blur: among all methods, they achieve the lowest standard deviation over the seven image sharpness levels; see the number next to each method in the legend of Fig. 6(a).

Joint visibility. While most 3DHPS methods assume that the target body is (almost) fully visible in the image, this is seldom the case in the first-person view images. To assess the importance of this issue, we analyze the performance of each baseline method with respect to the portion of visible body joints (“visibility”, see Sec. 4) in the images from our test set. The result is summarized in Fig. 6(b). Note that our definition of a joint’s visibility is related to, but differs from, the common concept of *occlusion*: both measure how much pixel information is missing for a body part, but visibility focuses on how much of the body is *truncated* from the image. A joint that is occluded by an object can still be considered visible by our definition.

Overall, all methods yield a lower error as the number of

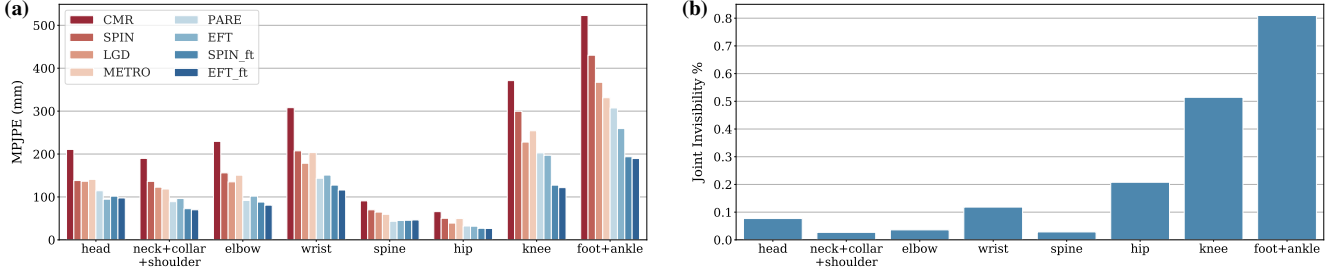


Figure 7. (a) 3D joint error analysis by body parts. (b) Ratio of each joint group being *invisible* (truncated) from the images in our test set.

visible body parts increases (*i.e.* less body truncation). Two recent methods, PARE [37] and EFT [29], achieve the best results. PARE is designed to be robust against occlusions by explicitly employing a body part attention mechanism, whereas EFT handles body truncation “implicitly” by aggressively cropping images as training data augmentation.

We further plot the MPJPE and the *invisibility* ratio of each joint group in Fig. 7. Overall the two are in accordance: the less frequent a joint is visible in the images, the higher error it has. An exception is on the wrist joints: despite good visibility, their error remains relatively high. As observed also in [37], high errors on the extremities are a common problem with existing 3DHPS models, possibly because most current models only use a single, global feature from the input image for regression. This points to potential future work that deploys local image features, which has been shown effective in recent 3DHPS models [21, 37].

5.3. Baseline Improvement

To evaluate the effectiveness of the EgoBody training set, we use it to fine-tune two of the baseline methods, SPIN [39] and EFT [29] as they both use the same architecture (HMR [33] network) that is the backbone for many other recent models [33, 36, 61]. The pre-trained EFT differs from SPIN majorly in that it is trained with extended 3D pseudo ground-truth data (from the EFT-dataset) and uses aggressive image cropping as data augmentation. We use the same hyperparameters provided by the authors and fine-tune the models for 25 epochs, where the validation loss plateaus (see Supp. Mat. for the training details).

As shown in Tab. 3, after fine-tuning, the error is largely reduced for both methods on all metrics: SPIN-ft has 49.3% lower MPJPE and 45.3% lower V2V error than the original SPIN model, whereas EFT-ft outperforms the original EFT by 25.0% and 19.7% on MPJPE and V2V, respectively. The improvement can also be seen for all blurriness/visibility categories in Figs. 6, 7. For the motion blur specifically, the fine-tuned models not only achieve a lower error at every image sharpness level, but also show an increased robustness. This is shown by the standard deviations (listed in Fig. 6) of each method across the sharpness levels, dropping from 21.46 to 7.78 for SPIN, and from 15.15 to 7.62 for EFT after fine-tuning.

Finally, we test SPIN and EFT against their fine-tuned counterparts on the You2Me [55] dataset. Here we report the PA-MPJPE for pose errors (in *mm*): SPIN (155.0) vs. SPIN-ft (89.4); and EFT (96.0) vs. EFT-ft (88.7). Again, fine-tuning on our training set improves both models’ performance; see Supp. Mat. for more details. These results suggest that our data is effective in helping existing models to address the challenges in egocentric view data.

6. Conclusion

We presented EgoBody, a dataset capturing social interactions in diverse environments. EgoBody collects multi-modal egocentric data, accompanied by ground-truth 3D human pose and shape for all interacting subjects. We define a benchmark and evaluate several state-of-the-art 3D human pose and shape estimation methods, showing their shortcomings on egocentric data. We also show that their performance can be enhanced by leveraging EgoBody’s annotations, providing insights for developing more robust methods for egocentric data. We consider EgoBody a first, much needed step towards better understanding human motion and social interactions in egocentric scenarios.

Limitations and future work. Currently our interactions are limited to the two-subject setup. In future work we will capture multi-people interactions and scale up the dataset further. Even richer data modalities (*e.g.* audio recordings and motion annotations by natural language descriptions) will potentially be included in future versions too.

Societal impact. EgoBody collects human data which can potentially contribute to negative trends (*e.g.* profit-driven personal data mining). We explicitly discussed this with the institutional ethics committee, which approved our proposal, and ensured a proper process to prevent misuses. Access to the data will be controlled and logged; each person who applies for the data will need to sign a license.

Acknowledgements. This work was supported by the Microsoft Mixed Reality & AI Zürich Lab PhD scholarship. Qianli Ma is partially funded by the Max Planck ETH Center for Learning Systems. We sincerely thank Samokhvalov Vyacheslav, Marko Mihajlovic, Sergey Prokudin, Shaofei Wang and Korrawe Karunratanakul for helping with the data capture and processing, and Taein Kwon, Jonas Hein for the discussion of the hardware setup.

We are grateful to Priyanka Patel, Muhammed Kocabas, Chun-Hao P. Huang, Vassilis Choutas, Timo Bolkart, Nikos Kolotouros, Lea Müller and Arjun Chandrasekaran for their valuable feedback and fruitful discussions. We thank Shaofei Wang, Francis Engelmann and Theodora Kontogianni for proof reading.

References

- [1] Azure Kinect. <https://docs.microsoft.com/en-us/azure/kinect-dk/>. 2, 4
- [2] Laan Labs 3D Scanner app. <https://apps.apple.com/us/app/3d-scanner-app/id1419913995>. 4
- [3] Microsoft HoloLens2. <https://www.microsoft.com/en-us/hololens>. 2, 4
- [4] Ankur Agarwal and Bill Triggs. Recovering 3D human pose from monocular images. *IEEE transactions on pattern analysis and machine intelligence*, 28(1):44–58, 2005. 3
- [5] Robert A. Nisbet. *The Social Bond: An Introduction to the Study of Society*. 1970. 2, 4
- [6] Alexandru O Bălan and Michael J Black. The naked truth: Estimating body shape under clothing. In *European Conference on Computer Vision*, pages 15–29. Springer, 2008. 3
- [7] P.J. Besl and Neil D. McKay. A method for registration of 3-d shapes. *IEEE Transactions on Pattern Analysis and Machine Intelligence*, 14(2):239–256, 1992. 1
- [8] Federica Bogo, Angjoo Kanazawa, Christoph Lassner, Peter Gehler, Javier Romero, and Michael J. Black. Keep it SMPL: Automatic estimation of 3D human pose and shape from a single image. In *European Conference on Computer Vision*, pages 561–578, 2016. 3
- [9] Z. Cao, G. Hidalgo Martinez, T. Simon, S. Wei, and Y. A. Sheikh. Openpose: Realtime multi-person 2d pose estimation using part affinity fields. *IEEE Transactions on Pattern Analysis and Machine Intelligence*, 2019. 5, 1
- [10] Hongsuk Choi, Gyeongsik Moon, Ju Yong Chang, and Kyoung Mu Lee. Beyond static features for temporally consistent 3d human pose and shape from a video. In *Proceedings of the IEEE/CVF Conference on Computer Vision and Pattern Recognition*, pages 1964–1973, 2021. 1, 3
- [11] Hongsuk Choi, Gyeongsik Moon, and Kyoung Mu Lee. Pose2Mesh: Graph convolutional network for 3d human pose and mesh recovery from a 2d human pose. In *European Conference on Computer Vision (ECCV)*, 2020. 3
- [12] Dima Damen, Hazel Doughty, Giovanni Maria Farinella, Sanja Fidler, Antonino Furnari, Evangelos Kazakos, Davide Moltisanti, Jonathan Munro, Toby Perrett, Will Price, et al. Scaling egocentric vision: The epic-kitchens dataset. In *Proceedings of the European Conference on Computer Vision (ECCV)*, pages 720–736, 2018. 2
- [13] Junting Dong, Qing Shuai, Yuanqing Zhang, Xian Liu, Xiaowei Zhou, and Hujun Bao. Motion capture from internet videos. In *European Conference on Computer Vision*, pages 210–227. Springer, 2020. 3
- [14] Qi Fang, Qing Shuai, Junting Dong, Hujun Bao, and Xiaowei Zhou. Reconstructing 3D human pose by watching humans in the mirror. In *Proceedings of the IEEE/CVF Conference on Computer Vision and Pattern Recognition*, pages 12814–12823, 2021. 1, 3
- [15] Alircza Fathi, Jessica K Hodgins, and James M Rehg. Social interactions: A first-person perspective. In *2012 IEEE Conference on Computer Vision and Pattern Recognition*, pages 1226–1233. IEEE, 2012. 2, 3
- [16] Mihai Fieraru, Mihai Zanfir, Elisabeta Oneata, Alin-Ionut Popa, Vlad Olaru, and Cristian Sminchisescu. Three-dimensional reconstruction of human interactions. In *Proceedings of the IEEE/CVF Conference on Computer Vision and Pattern Recognition*, pages 7214–7223, 2020. 2
- [17] Juergen Gall, Bodo Rosenhahn, Thomas Brox, and Hans-Peter Seidel. Optimization and filtering for human motion capture. *International journal of computer vision*, 87(1-2):75, 2010. 3
- [18] John C Gower. Generalized procrustes analysis. *Psychometrika*, 40(1):33–51, 1975. 7
- [19] Kristen Grauman et al. Ego4D: Around the world in 3000 hours of egocentric video. *arXiv preprint arXiv:2110.07058*, 2021. 3
- [20] Kristen Grauman, Gregory Shakhnarovich, and Trevor Darrell. Inferring 3D structure with a statistical image-based shape model. In *ICCV*, volume 3, page 641, 2003. 3
- [21] Riza Alp Guler and Iasonas Kokkinos. Holopose: Holistic 3D human reconstruction in-the-wild. In *Proceedings of the IEEE Conference on Computer Vision and Pattern Recognition*, pages 10884–10894, 2019. 3, 8
- [22] Vladimir Guzov, Aymen Mir, Torsten Sattler, and Gerard Pons-Moll. Human positioning system (HPS): 3D human pose estimation and self-localization in large scenes from body-mounted sensors. In *Proceedings of the IEEE/CVF Conference on Computer Vision and Pattern Recognition*, pages 4318–4329, 2021. 2, 3, 1
- [23] Mohamed Hassan, Vasileios Choutas, Dimitrios Tzionas, and Michael J Black. Resolving 3D human pose ambiguities with 3D scene constraints. In *Proceedings of the IEEE/CVF International Conference on Computer Vision*, pages 2282–2292, 2019. 1, 2, 3, 5
- [24] Kaiming He, Georgia Gkioxari, Piotr Dollár, and Ross Girshick. Mask r-cnn. In *Proceedings of the IEEE international conference on computer vision*, pages 2961–2969, 2017. 5, 1
- [25] Alejandro Hernandez, Jurgen Gall, and Francesc Moreno-Noguer. Human motion prediction via spatio-temporal inpainting. In *Proceedings of the IEEE/CVF International Conference on Computer Vision*, pages 7134–7143, 2019. 1
- [26] Yinghao Huang, Federica Bogo, Christoph Lassner, Angjoo Kanazawa, Peter V Gehler, Javier Romero, Ijaz Akhter, and Michael J Black. Towards accurate marker-less human shape and pose estimation over time. In *2017 international conference on 3D vision (3DV)*, pages 421–430. IEEE, 2017. 3
- [27] Catalin Ionescu, Dragos Papava, Vlad Olaru, and Cristian Sminchisescu. Human3.6m: Large scale datasets and predictive methods for 3d human sensing in natural environments. *IEEE transactions on pattern analysis and machine intelligence*, 36(7):1325–1339, 2013. 2, 3, 6
- [28] Hao Jiang and Kristen Grauman. Seeing invisible poses: Estimating 3d body pose from egocentric video. In *2017 IEEE Conference on Computer Vision and Pattern Recognition (CVPR)*, pages 3501–3509. IEEE, 2017. 3
- [29] Hanbyul Joo, Natalia Neverova, and Andrea Vedaldi. Exemplar fine-tuning for 3D human pose fitting towards in-the-wild 3d human pose estimation. 2021. 2, 3, 6, 7, 8

- [30] Hanbyul Joo, Tomas Simon, Mina Cikara, and Yaser Sheikh. Towards social artificial intelligence: Nonverbal social signal prediction in a triadic interaction. In *Proceedings of the IEEE/CVF Conference on Computer Vision and Pattern Recognition*, pages 10873–10883, 2019. **2**
- [31] Hanbyul Joo, Tomas Simon, Xulong Li, Hao Liu, Lei Tan, Lin Gui, Sean Banerjee, Timothy Godisart, Bart Nabbe, Iain Matthews, et al. Panoptic studio: A massively multiview system for social interaction capture. *IEEE transactions on pattern analysis and machine intelligence*, 41(1):190–204, 2017. **2, 3**
- [32] Hanbyul Joo, Tomas Simon, and Yaser Sheikh. Total capture: A 3D deformation model for tracking faces, hands, and bodies. In *Proceedings of the IEEE conference on computer vision and pattern recognition*, pages 8320–8329, 2018. **2, 3**
- [33] Angjoo Kanazawa, Michael J Black, David W Jacobs, and Jitendra Malik. End-to-end recovery of human shape and pose. In *Proceedings of the IEEE Conference on Computer Vision and Pattern Recognition*, pages 7122–7131, 2018. **1, 3, 8**
- [34] Angjoo Kanazawa, Jason Y Zhang, Panna Felsen, and Jitendra Malik. Learning 3D human dynamics from video. In *Proceedings of the IEEE Conference on Computer Vision and Pattern Recognition*, pages 5614–5623, 2019. **1, 3**
- [35] Will Kay, Joao Carreira, Karen Simonyan, Brian Zhang, Chloe Hillier, Sudheendra Vijayanarasimhan, Fabio Viola, Tim Green, Trevor Back, Paul Natsev, et al. The kinetics human action video dataset. *arXiv preprint arXiv:1705.06950*, 2017. **2**
- [36] Muhammed Kocabas, Nikos Athanasiou, and Michael J Black. VIBE: Video inference for human body pose and shape estimation. In *Proceedings of the IEEE/CVF Conference on Computer Vision and Pattern Recognition*, pages 5253–5263, 2020. **1, 3, 8**
- [37] Muhammed Kocabas, Chun-Hao P. Huang, Otmar Hilliges, and Michael J. Black. PARE: Part attention regressor for 3D human body estimation. In *Proceedings International Conference on Computer Vision (ICCV)*, pages 11127–11137. IEEE, Oct. 2021. **3, 7, 8, 2**
- [38] Muhammed Kocabas, Chun-Hao P. Huang, Joachim Tesch, Lea Müller, Otmar Hilliges, and Michael J. Black. SPEC: Seeing people in the wild with an estimated camera. In *Proc. International Conference on Computer Vision (ICCV)*, pages 11035–11045, Oct. 2021.
- [39] Nikos Kolotouros, Georgios Pavlakos, Michael J Black, and Kostas Daniilidis. Learning to reconstruct 3D human pose and shape via model-fitting in the loop. In *Proceedings of the IEEE International Conference on Computer Vision*, pages 2252–2261, 2019. **1, 2, 3, 6, 7, 8**
- [40] Nikos Kolotouros, Georgios Pavlakos, and Kostas Daniilidis. Convolutional mesh regression for single-image human shape reconstruction. In *CVPR*, 2019. **7**
- [41] Nikos Kolotouros, Georgios Pavlakos, Dinesh Jayaraman, and Kostas Daniilidis. Probabilistic modeling for human mesh recovery. In *ICCV*, 2021. **3**
- [42] Taein Kwon, Bugra Tekin, Jan Stuhmer, Federica Bogo, and Marc Pollefeys. H2O: Two hands manipulating objects for first person interaction recognition. In *International Conference on Computer Vision (ICCV)*, 2021. **2**
- [43] CMU Graphics Lab. CMU Graphics Lab Motion Capture Database. <http://mocap.cs.cmu.edu/>, 2000. **2**
- [44] Jiefeng Li, Chao Xu, Zhicun Chen, Siyuan Bian, Lixin Yang, and Cewu Lu. HybrIK: A hybrid analytical-neural inverse kinematics solution for 3d human pose and shape estimation. In *Proceedings of the IEEE/CVF Conference on Computer Vision and Pattern Recognition*, pages 3383–3393, 2021. **3**
- [45] Yin Li, Miao Liu, and James M Rehg. In the eye of beholder: Joint learning of gaze and actions in first person video. In *Proceedings of the European Conference on Computer Vision (ECCV)*, pages 619–635, 2018. **2**
- [46] Kevin Lin, Lijuan Wang, and Zicheng Liu. End-to-end human pose and mesh reconstruction with transformers. In *CVPR*, 2021. **3, 7**
- [47] Miao Liu, Dexin Yang, Yan Zhang, Zhaopeng Cui, James M Rehg, and Siyu Tang. 4D human body capture from egocentric video via 3D scene grounding. *2021 international conference on 3D vision (3DV)*, 2021. **2, 3**
- [48] Matthew Loper, Naureen Mahmood, Javier Romero, Gerard Pons-Moll, and Michael J Black. SMPL: A skinned multi-person linear model. *ACM transactions on graphics (TOG)*, 34(6):1–16, 2015. **2, 3**
- [49] Zhengyi Luo, S Alireza Golestaneh, and Kris M Kitani. 3D human motion estimation via motion compression and refinement. In *Proceedings of the Asian Conference on Computer Vision*, 2020. **1, 3**
- [50] Zhengyi Luo, Ryo Hachiuma, Ye Yuan, Shun Iwase, and Kris M Kitani. Kinematics-guided reinforcement learning for object-aware 3d ego-pose estimation. *arXiv preprint arXiv:2011.04837*, 2020. **3**
- [51] Naureen Mahmood, Nima Ghorbani, Nikolaus F Troje, Gerard Pons-Moll, and Michael J Black. AMASS: Archive of motion capture as surface shapes. In *Proceedings of the IEEE/CVF International Conference on Computer Vision*, pages 5442–5451, 2019. **2, 1**
- [52] Dushyant Mehta, Helge Rhodin, Dan Casas, Pascal Fua, Oleksandr Sotnychenko, Weipeng Xu, and Christian Theobalt. Monocular 3D human pose estimation in the wild using improved cnn supervision. In *2017 international conference on 3D vision (3DV)*, pages 506–516. IEEE, 2017. **2**
- [53] Gyeongsik Moon and Kyoung Mu Lee. I2L-MeshNet: Image-to-lixel prediction network for accurate 3d human pose and mesh estimation from a single rgb image. In *European Conference on Computer Vision (ECCV)*, 2020. **3**
- [54] Sanath Narayan, Mohan S Kankanhalli, and Kalpathi R Ramakrishnan. Action and interaction recognition in first-person videos. In *Proceedings of the IEEE Conference on Computer Vision and Pattern Recognition Workshops*, pages 512–518, 2014. **2, 3**
- [55] Evonne Ng, Donglai Xiang, Hanbyul Joo, and Kristen Grauman. You2me: Inferring body pose in egocentric video via first and second person interactions. In *Proceedings of the IEEE/CVF Conference on Computer Vision and Pattern Recognition*, pages 9890–9900, 2020. **2, 3, 6, 8**
- [56] Mohamed Omran, Christoph Lassner, Gerard Pons-Moll, Peter Gehler, and Bernt Schiele. Neural body fitting: Unifying deep learning and model based human pose and shape estimation. In *2018 international conference on 3D vision (3DV)*, pages 484–494. IEEE, 2018. **3**
- [57] Priyanka Patel, Chun-Hao P. Huang, Joachim Tesch,

- David T. Hoffmann, Shashank Tripathi, and Michael J. Black. AGORA: Avatars in geography optimized for regression analysis. In *Proceedings IEEE/CVF Conf. on Computer Vision and Pattern Recognition (CVPR)*, June 2021. 2, 6, 7
- [58] Georgios Pavlakos, Vasileios Choutas, Nima Ghorbani, Timo Bolkart, Ahmed AA Osman, Dimitrios Tzionas, and Michael J Black. Expressive body capture: 3D hands, face, and body from a single image. In *Proceedings of the IEEE Conference on Computer Vision and Pattern Recognition*, pages 10975–10985, 2019. 1, 2, 3, 4
- [59] José Luis Pech-Pacheco, Gabriel Cristóbal, Jesús Chamorro-Martínez, and Joaquín Fernández-Valdivia. Diatom auto-focusing in brightfield microscopy: a comparative study. In *Proceedings 15th International Conference on Pattern Recognition. ICPR-2000*, volume 3, pages 314–317. IEEE, 2000. 7, 2
- [60] Hamed Pirsiavash and Deva Ramanan. Detecting activities of daily living in first-person camera views. In *2012 IEEE conference on computer vision and pattern recognition*, pages 2847–2854. IEEE, 2012. 2
- [61] Yu Rong, Takaaki Shiratori, and Hanbyul Joo. FrankMocap: A monocular 3d whole-body pose estimation system via regression and integration. In *IEEE International Conference on Computer Vision Workshops*, 2021. 8
- [62] Michael S Ryoo and Larry Matthies. First-person activity recognition: What are they doing to me? In *Proceedings of the IEEE conference on computer vision and pattern recognition*, pages 2730–2737, 2013. 2, 3
- [63] Nitin Saini, Eric Price, Rahul Tallamraju, Raffi Enfi-
aud, Roman Ludwig, Igor Martinovic, Aamir Ahmad, and Michael J Black. Markerless outdoor human motion capture using multiple autonomous micro aerial vehicles. In *Proceedings of the IEEE/CVF International Conference on Computer Vision*, pages 823–832, 2019. 3
- [64] Takaaki Shiratori, Hyun Soo Park, Leonid Sigal, Yaser Sheikh, and Jessica K Hodgins. Motion capture from body-mounted cameras. In *ACM SIGGRAPH 2011 papers*, pages 1–10. 2011. 3
- [65] Gunnar A Sigurdsson, Abhinav Gupta, Cordelia Schmid, Ali Farhadi, and Karteek Alahari. Actor and observer: Joint modeling of first and third-person videos. In *Proceedings of the IEEE Conference on Computer Vision and Pattern Recognition*, pages 7396–7404, 2018. 2
- [66] Jie Song, Xu Chen, and Otmar Hilliges. Human body model fitting by learned gradient descent. 2020. 3, 7
- [67] Yu Sun, Yun Ye, Wu Liu, Wenpeng Gao, YiLi Fu, and Tao Mei. Human mesh recovery from monocular images via a skeleton-disentangled representation. In *Proceedings of the IEEE International Conference on Computer Vision*, pages 5349–5358, 2019. 1, 3
- [68] Jun Kai Vince Tan, Ignas Budvytis, and Roberto Cipolla. Indirect deep structured learning for 3D human body shape and pose prediction. 2017. 3
- [69] Denis Tome, Thiemo Alldieck, Patrick Peluse, Gerard Pons-Moll, Lourdes Agapito, Hernan Badino, and Fernando De la Torre. Selfpose: 3D egocentric pose estimation from a headset mounted camera. *arXiv preprint arXiv:2011.01519*, 2020. 2, 3
- [70] Denis Tome, Patrick Peluse, Lourdes Agapito, and Hernan Badino. xr-egopose: Egocentric 3d human pose from an hmd camera. In *Proceedings of the IEEE/CVF International Conference on Computer Vision*, pages 7728–7738, 2019. 2, 3
- [71] Matt Trumble, Andrew Gilbert, Charles Malleon, Adrian Hilton, and John Collomosse. Total capture: 3d human pose estimation fusing video and inertial sensors. In *2017 British Machine Vision Conference (BMVC)*, 2017. 2, 3
- [72] Hsiao-Yu Tung, Hsiao-Wei Tung, Ersin Yumer, and Katerina Fragkiadaki. Self-supervised learning of motion capture. In *Advances in Neural Information Processing Systems*, pages 5236–5246, 2017. 3
- [73] Dorin Ungureanu, Federica Bogo, Silvano Galliani, Pooja Sama, Xin Duan, Casey Meekhof, Jan Stuhmer, Thomas J. Cashman, Bugra Tekin, Johannes L. Schonberger, Bugra Tekin, Pawel Olszta, and Marc Pollefeys. HoloLens 2 Research Mode as a Tool for Computer Vision Research. *arXiv:2008.11239*, 2020. 4, 3
- [74] Timo von Marcard, Roberto Henschel, Michael J Black, Bodo Rosenhahn, and Gerard Pons-Moll. Recovering accurate 3d human pose in the wild using imus and a moving camera. In *Proceedings of the European Conference on Computer Vision (ECCV)*, pages 601–617, 2018. 2, 3, 6, 7
- [75] Timo von Marcard, Gerard Pons-Moll, and Bodo Rosenhahn. Human pose estimation from video and IMUs. *Transactions on Pattern Analysis and Machine Intelligence*, 38(8):1533–1547, Jan. 2016. 2, 3
- [76] Bastian Wandt, Marco Rudolph, Petriša Zell, Helge Rhodin, and Bodo Rosenhahn. CanonPose: Self-supervised monocular 3d human pose estimation in the wild. In *Proceedings of the IEEE/CVF Conference on Computer Vision and Pattern Recognition*, pages 13294–13304, 2021. 3
- [77] Yangang Wang, Yebin Liu, Xin Tong, Qionghai Dai, and Ping Tan. Outdoor markerless motion capture with sparse handheld video cameras. *IEEE transactions on visualization and computer graphics*, 24(5):1856–1866, 2017. 3
- [78] Zhenzhen Weng and Serena Yeung. Holistic 3D human and scene mesh estimation from single view images. In *Proceedings of the IEEE/CVF Conference on Computer Vision and Pattern Recognition*, pages 334–343, 2021. 1, 3
- [79] Donglai Xiang, Hanbyul Joo, and Yaser Sheikh. Monocular total capture: Posing face, body, and hands in the wild. In *Proceedings of the IEEE/CVF Conference on Computer Vision and Pattern Recognition*, 2019. 2
- [80] Weipeng Xu, Avishek Chatterjee, Michael Zollhoefer, Helge Rhodin, Pascal Fua, Hans-Peter Seidel, and Christian Theobalt. Mo2Cap2: Real-time mobile 3D motion capture with a cap-mounted fisheye camera. *IEEE transactions on visualization and computer graphics*, 25(5):2093–2101, 2019. 2, 3
- [81] Yuanlu Xu, Song-Chun Zhu, and Tony Tung. Denserac: Joint 3D pose and shape estimation by dense render-and-compare. In *Proceedings of the IEEE/CVF International Conference on Computer Vision*, pages 7760–7770, 2019. 1, 3
- [82] Zhefan Ye, Yin Li, Yun Liu, Chanel Bridges, Agata Rozga, and James M Rehg. Detecting bids for eye contact using a wearable camera. In *2015 11th IEEE International Conference and Workshops on Automatic Face and Gesture Recognition (FG)*, volume 1, pages 1–8. IEEE, 2015. 3
- [83] Ryo Yonetani, Kris M Kitani, and Yoichi Sato. Recognizing micro-actions and reactions from paired egocentric videos.

- In *Proceedings of the IEEE Conference on Computer Vision and Pattern Recognition*, pages 2629–2638, 2016. 2, 3
- [84] Zhixuan Yu, Jae Shin Yoon, In Kyu Lee, Prashanth Venkatesh, Jaesik Park, Jihun Yu, and Hyun Soo Park. Humbi: A large multiview dataset of human body expressions. In *Proceedings of the IEEE/CVF Conference on Computer Vision and Pattern Recognition*, pages 2990–3000, 2020. 2, 3
- [85] Ye Yuan and Kris Kitani. Ego-pose estimation and forecasting as real-time pd control. In *Proceedings of the IEEE/CVF International Conference on Computer Vision*, pages 10082–10092, 2019. 2, 3
- [86] Ye Yuan, Shih-En Wei, Tomas Simon, Kris Kitani, and Jason Saragih. Simpoe: Simulated character control for 3d human pose estimation. In *Proceedings of the IEEE/CVF Conference on Computer Vision and Pattern Recognition*, pages 7159–7169, 2021. 1, 3
- [87] Andrei Zanfir, Eduard Gabriel Bazavan, Hongyi Xu, Bill Freeman, Rahul Sukthankar, and Cristian Sminchisescu. Weakly supervised 3D human pose and shape reconstruction with normalizing flows. *arXiv preprint arXiv:2003.10350*, 2020. 3
- [88] Jianfeng Zhang, Dongdong Yu, Jun Hao Liew, Xuecheng Nie, and Jiashi Feng. Body meshes as points. In *Proceedings of the IEEE/CVF Conference on Computer Vision and Pattern Recognition*, pages 546–556, 2021. 3
- [89] Siwei Zhang, Yan Zhang, Federica Bogo, Pollefeys Marc, and Siyu Tang. Learning motion priors for 4D human body capture in 3D scenes. In *International Conference on Computer Vision (ICCV)*, Oct. 2021. 1, 2, 3, 4, 5
- [90] Yuxiang Zhang, Liang An, Tao Yu, Xiu Li, Kun Li, and Yebin Liu. 4D association graph for realtime multi-person motion capture using multiple video cameras. In *Proceedings of the IEEE/CVF Conference on Computer Vision and Pattern Recognition*, pages 1324–1333, 2020. 2
- [91] Yuxiao Zhou, Marc Habermann, Ikhsanul Habibie, Ayush Tewari, Christian Theobalt, and Feng Xu. Monocular real-time full body capture with inter-part correlations. In *Proceedings of the IEEE/CVF Conference on Computer Vision and Pattern Recognition*, pages 4811–4822, 2021. 3

EgoBody: Human Body Shape, Motion and Social Interactions from Head-Mounted Devices

Supplementary Material

A. Details of Dataset Building

A.1. Calibration

To spatially calibrate the Kinects-Kinects and Kinects-Hololens2, we employ a checkerboard to obtain an initial calibration; we then refine the result by running ICP [7] on the scene point clouds reconstructed from the depth sensor of the devices. To register camera data into the 3D scene, we first manually annotate a set of correspondence points between the scene mesh and scene point clouds given by the Kinect depth frames to obtain an initial rigid transformation, which again is refined via ICP.

A.2. Data Processing

Body point cloud extraction. We firstly use MaskRCNN [24] to get coarse human instance segmentation masks in Kinect RGB frames and refine the masks with DeepLabv3 [24]. The obtained human instance segmentation masks are mapped to Kinect depth frames to segment the human body point clouds from point clouds extracted from depth.

Subject index reordering. Note that OpenPose [9], MaskRCNN and DeepLabv3 all work per-frame, without temporal tracking. For each sequence, we therefore reorder subject indices from OpenPose detections and human masks by their relative position to each other in 2D, such that each subject has a consistent index across all frames and all Kinect views.

Data cleaning. 2D joint detection and human instance segmentation can fail in the presence of body-body or body-scene occlusions (Fig. S1 left/middle). Thus we manually clean the failed detections and exclude them from the reconstruction pipeline. We also manually clean inaccurate 2D joint detections due to self-occlusions (Fig. S1 right).

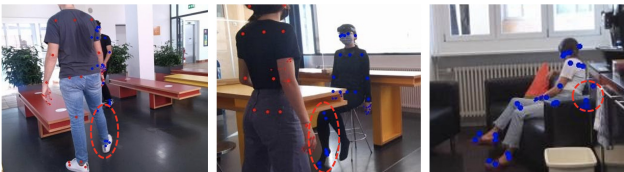


Figure S1. Limitations for OpenPose 2D joint detection when body-body occlusion (left), body-scene occlusion (middle), or self-occlusion (right) happens. Different keypoint colors denote different detected body indices.

EgoSet-second-person subset selecting. Egocentric image frames with extreme human body truncations are excluded from EgoSet-second-person subset by the following filtering procedure. We run OpenPose 2D joint detection on all egocentric image frames, and manually exclude spurious detections (irrelevant people in the background or false positives on scene objects) for each frame. As OpenPose may split the joints from the same body into several detections, we merge them into one body in such case, where the joint conflict is resolved by the confidence score. We include the frames in EgoSet-second-person subset when at least 6 valid joints (OpenPose BODY_25 format) of the second person are detected. We threshold the joint confidence score by 0.2 as in [39]. Note that 5 joints concentrated on the head are considered as one joint due to the close distances, as well as the 4 joints on each foot. The bounding box is computed with the processed results.

B. Motion Smoothness

Following [89], the motion smoothness of our dataset is evaluated by the Power Spectrum KL divergence score (PSKL) [25], by measuring the acceleration distribution distance between our dataset and the high quality mocap dataset AMASS [51]. The lower the score is, the more the motions resemble the natural motions in AMASS dataset. Besides, we also compare with HPS [22], a recent egocentric view dataset (see Tab. S1). Our dataset achieves significant better motion smoothness score than the HPS dataset, demonstrating the high quality of the ground truth motions.

C. More Statistics

Joint invisibility. We consider 2 types of “invisibility” measurements: frame-wise invisibility and joint-wise invisibility ratio. For each frame, the frame-wise invisibility ratio calculates the percentage of invisible joints among all

Table S1. Motion smoothness evaluation of our dataset and the HPS dataset. $PSKL(X, A)$ denotes $PSKL(HPS/ours, AMASS)$, and $PSKL(A, HPS/ours)$ the reverse direction. The better result is in boldface.

	$PSKL(X, A) \downarrow$	$PSKL(A, X) \downarrow$
HPS [22]	0.924	1.044
EgoBody (ours)	0.401	0.348

body joints. As shown in Fig. S2(a), partial body invisibility occurs in most frames, with even over 60% body joints invisible in extreme cases. For each body joint, the joint-wise invisibility ratio calculates the ratio of frames when the joint is invisible among all frames (See Fig. S2(b)). The lower part of the body exhibits higher chances of invisibility (knees around 50% and feet around 80%). The upper body parts are more visible: neck, shoulder, spine, and elbow joints above all, while wrist and head joints have slightly higher invisibility (around 10%).

Eye gaze and attention. The HoloLens2 eye tracking provides the eye gaze 3D ray’s starting point and orientation, which we can intersect with our 3D reconstructions to calculate the location the user looks at. By projecting the 3D eye gaze point onto the egocentric images, we perform analysis on the distances between this projected 2D eye gaze point (attention area) and the body joints of the *second person* on the first-person view images. For all frames where the 2D gaze point lies within the image, the mean Euclidean distance between the 2D gaze point and its nearest body joint is 126.22 (pixels): Fig. S3(a) plots the distribution. For more than 75% of the frames, the distance between the 2D gaze point and its nearest joint lies within 120 (pixels), indicating that the camera wearer’s attention is highly focused on the *second person* during interactions. The mean distance between each joint and the 2D gaze point over all frames (Fig. S3(b)) reveals that the subjects’ attention tends to be closer to the upper body joints during interactions.

Interaction distance. Fig. S4(a) shows the distribution of the interaction distances between 2 interacting subjects. The diverse interactions and indoor scenes allow a large coverage of the interaction distances.

Motion blur. The image sharpness score (variance of the Laplacian of the image) [59] quantifies the motion blur in our dataset (the distribution is shown in Fig. S4(b)). A higher score indicates sharper images.

D. Experiments: Details and Discussions

Discussion on evaluation metrics. While MPJPE is a commonly used measurement for pose estimation accuracy, it is very sparse and does not penalize the error caused by wrong joint twisting. This motivates us to also include the V2V error as a metric in our benchmark: it is not only a straightforward measure for the shape estimation, but also measures the pose error in a denser and stricter way than MPJPE as it also penalizes erroneous longitudinal joint rotations.

By default we consider the MPJPE and the V2V errors without the Procrustes Alignment (PA), as PA eliminates the discrepancy in the global orientation, a major source of errors for most methods. Deprecating PA-based metrics is

becoming a recent trend [37, 57]. Note that we evaluate MPJPE on 22 joints that are in common between SMPL (the format of the baseline results) and SMPL-X (our ground truth); *i.e.* we use all body joints from SMPL except for the 2 hand joints.

D.1. Baseline Improvement on EgoBody

Implementation details. We fine-tune SPIN and EFT using the official codes, but with slight customization in the training as follows. For SPIN, we disable the SMPLify-in-the-loop during training since the EgoBody training set already provides direct 3D supervision from the pseudo ground truth. Note that this is in fact the default setting in SPIN when the 3D ground truth is available. The fine-tune stops at 25 epochs when the validation loss becomes stable.

Extended results and discussions. As shown in Fig. S6, while SPIN works well on images when the full body is visible, it fails on images where the subjects are truncated. EFT, in contrast, is more robust against such truncation as the model is trained on aggressively cropped images as data augmentation during training. The effectiveness of EFT’s data augmentation is further supported by our fine-tuning experiments. After fine tuning SPIN and EFT on our training set, both models show greater robustness against motion blur and image truncation, and quantitatively achieve lower errors than the original models on all metrics, as shown in the main paper Tab. 3. Together with the experiments on the You2Me dataset (see main paper Sec. 5.3), this shows that our training set can help adapt existing 3DHPS models to egocentric view data.

D.2. Baseline Improvement on the You2Me Dataset

Here we report the experimental setup of the You2Me dataset experiment. The You2Me dataset [55] provides egocentric view images (taken with a chest-mounted GoPro camera), and the ground truth 3D joint locations of both the camera wearer and the *second person* (*i.e.* the subject in the egocentric view whose body pose and shape is to be estimated). The provided ground truth 3D joints are however in a world coordinate system, making it infeasible to compute the translation-only MPJPE (see main paper Sec. 5.1): since the camera calibration between the GoPro and the world coordinate is unknown, even a perfect prediction (in the camera coordinate system) may differ from the ground truth up to a rigid transformation. To account for this problem, we first perform the Procrustes Alignment, which solves for the scale, translation and global rotation, to align the predicted 3D body joints with the ground truth, and then compute the MPJPE of the aligned bodies, resulting in the PA-MPJPE errors reported in the paper.

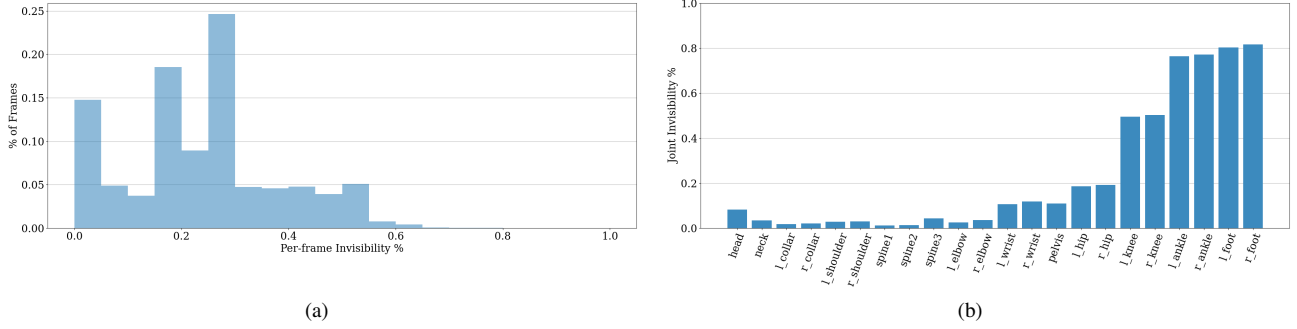


Figure S2. (a) Distribution of frame-wise invisibility ratio (% of invisible joints among all body joints for each frame). (b) Joint-wise invisibility ratio (% of occurrences when the corresponding joint is invisible among all frames.): ‘L.’ denotes ‘left.’ and ‘r.’ denotes ‘right.’.

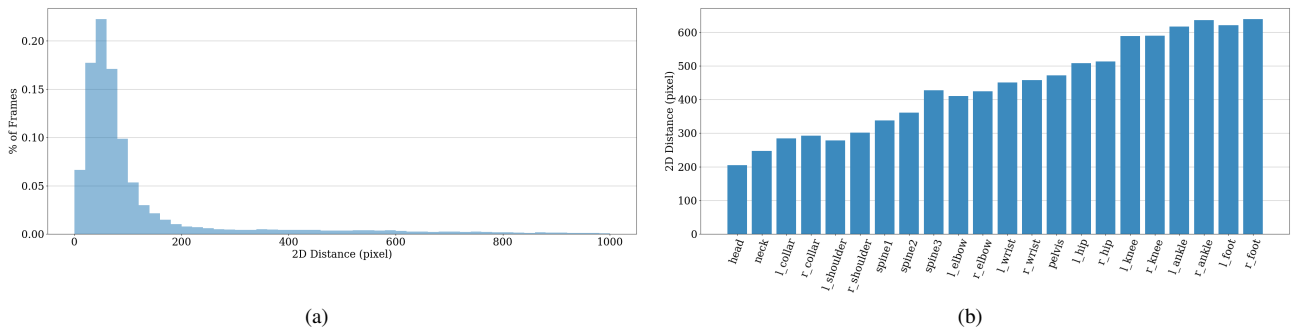


Figure S3. (a) Distribution of the 2D distance between the 2D gaze point and its nearest body joint. (b) Mean 2D distance between the 2D gaze point and each body joint. ‘L.’ denotes ‘left.’ and ‘r.’ denotes ‘right.’.

E. AMT Annotation Details

To evaluate the body shape and pose annotation accuracy, we collect manual annotations of 2D locations of 17 body joints on the EgoSet-*second-person* frames via Amazon Mechanical Turk (AMT). The user interface is illustrated in Fig. S7(a). We exclude body joints that are ambiguous for manual annotating (head, spine1, spine2, spine3, left_collar, right_collar) from the first 22 SMPL-X body joints, and add the nose joint which is easy to define for users. The user is provided with the definition of body joints (Fig. S7(b)), and an image of the target person to annotate (in case of irrelevant people in the background). Self-occluded keypoints need to be inferred, while keypoints occluded by scene objects are not required to be annotated. We downsample with a rate of 50 on the EgoSet-*second-person* data, which yields a total number of 2286 frames.

For better annotation quality, each frame is annotated by 5 users, and joints annotated by less than three users are ignored. A small part of the users flip the left and right side, inducing non-negligible noise for the ground-truth evaluation. To address this issue, we filter out the outliers and correct the flipped annotations by the following procedure. For each annotated joint, the 2D distance from each annotation \mathbf{x}_i ($i = 0, 1, \dots, 4$) to the mean location $\bar{\mathbf{x}}$ is calculated

as $d_i = \|\mathbf{x}_i - \bar{\mathbf{x}}\|_2$. An annotation is considered as the outlier if $\frac{d_i - \bar{d}}{\sigma} > 1.5$, where \bar{d} is the average distance, and $\sigma = \sqrt{\frac{1}{n}(d_i - \bar{d})^2}$ is the standard deviation of the distance. For joints that have the counterpart on the other side of body we flip the left/right side of the annotations and perform the same outlier detection, to fix cases when the users flip the left and right side.

F. Limitations

As there exists no solution to synchronize HoloLens2 and Kinect via hardware, we align their clocks via software, using a flashlight which is visible to all devices as signal for the first frame. Although HoloLens2 exhibit frame drops occasionally, the corresponding frames of all devices can be aligned according to the timestamps provided by HoloLens2 Research Mode API [73]. Besides, we empirically observe a small temporal misalignment. In our case, the misalignment can be observed for fast motions (for example, for hand movements, as shown in Fig. S5). However, this issue is inevitable for the synchronization between third-person view cameras and HMDs [22, 55]. Despite the small misalignment, our reconstruction reaches a high accuracy as proved by the reconstruction accuracy in Sec. 3.

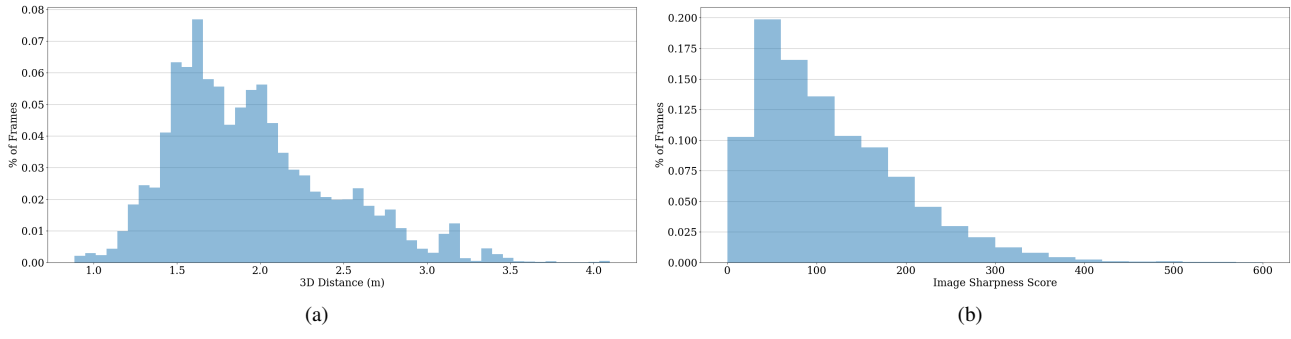


Figure S4. (a) Distribution of interaction distances between 2 interacting subjects. (b) Distribution of the image sharpness score on EgoSet-second-person test set.



Figure S5. Misalignments between the body mesh and HoloLens2 images during fast motions (for example, fast hand movements).

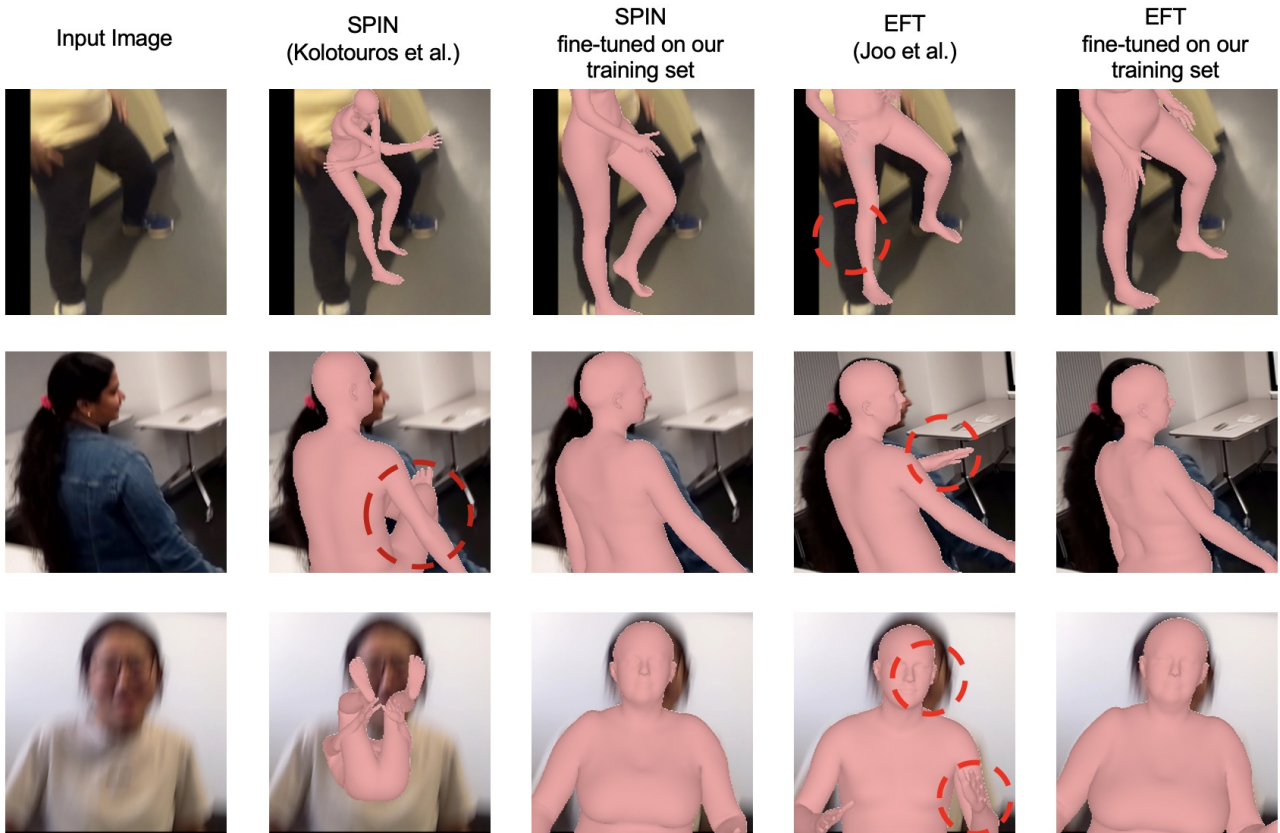
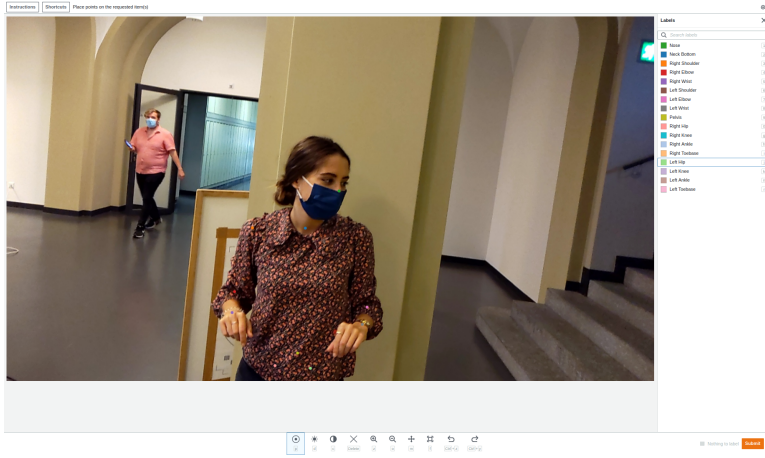
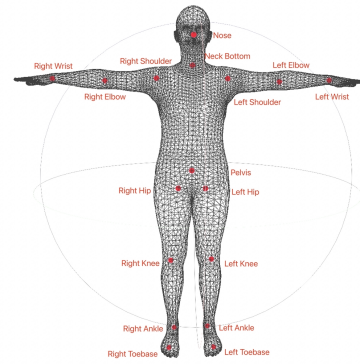


Figure S6. Qualitative results from the baseline evaluation.



(a)



(b)

Figure S7. (a) The user interface, and the (b) definition of the 17 joints, for AMT manual annotation.